

000 001 002 003 004 005 PROSAFEPRUNE: PROJECTED SAFETY PRUNING FOR 006 MITIGATING OVER-REFUSAL IN LLMs 007 008 009

010 **Anonymous authors**
011 Paper under double-blind review
012
013
014
015
016
017
018
019
020
021
022
023
024
025
026
027
028
029
030
031
032
033
034
035
036
037
038
039
040
041
042
043
044
045
046
047
048
049
050
051
052
053

ABSTRACT

Large Language Models (LLMs) excel in various domains, but their safe deployment faces the challenge of balancing safety and utility. Existing alignment strategies often strengthen refusal mechanisms to reduce harmful outputs, but harmless instructions with superficial risky words are mistakenly rejected, which is known as *over-refusal*. This work first reveals that over-refusal stems from a *cognitive bias* in the model’s internal representation space: LLMs naturally encode safety attributes in hidden states, and pseudo-harmful instructions overlap with harmful features, causing over-harmful encoding. To address this, we propose ProSafePrune, a subspace-projected low-rank parameter pruning framework for mitigating LLM over-refusal. By projecting pseudo-harmful features into subspaces and removing low-rank directions corresponding to harmful components in the most discriminative layers, we significantly reduce over-refusal while preserving the model’s ability to reject genuinely harmful requests, improving performance on general tasks. In experiments, across different models, our method significantly lowers the average false rejection rate while slightly improving general task performance.

1 INTRODUCTION

Large Language Models (LLMs) achieve strong performance across domains, yet their safe deployment hinges on balancing safety and usefulness (Bai et al., 2022; Bianchi et al., 2023; Dai et al., 2023; Huang et al., 2024; Zou et al., 2024). Current alignment practices typically strengthen refusal mechanisms to suppress harmful outputs, but this often results in over-refusal (Röttger et al., 2023; Zhang et al., 2025)—rejecting not only genuinely harmful requests but also harmless ones that merely contain superficially risky cues. This undermines usability and has long been viewed as a side effect of overly conservative alignment.

Building on this observation, prior research has explored two main lines of mitigation. Training-based methods (Zhang et al., 2024; Zheng et al., 2024; Dabas et al., 2025) can be effective, but they demand additional data and computation, limiting practicality. Training-free methods (Cao et al., 2025; Shi et al., 2024) provide greater flexibility, yet they often fail to resolve the underlying bias and frequently introduce extra inference-time overhead. These limitations highlight the need for an approach that is both lightweight and able to directly address the root cause of over-refusal.

In contrast, we firstly reveal that over-refusal is not merely a failure of existing alignment pipelines, but rather a manifestation of an inherent *cognitive bias* in the model’s internal representation space. Prior studies have shown that hidden states of LLMs naturally encode safety attributes of input instructions (Li et al., 2024; Zhao et al., 2025). However, pseudo-harmful instructions often project simultaneously onto both the harmful subspace and the harmless subspace. Under excessive safety fine-tuning, this natural overlap becomes distorted: the harmful projection is disproportionately amplified while the harmless one is suppressed. As a result, benign instructions are over-encoded with harmful features, shifting the internal decision boundary and ultimately leading to false rejections. Interestingly, this phenomenon—which we term *over-harmful encoding*—also provides insight into the origin of the alignment tax (Huang et al., 2025), where models are pushed into an overly cautious regime that further constrains their general task performance.

In this work, we introduce a new perspective for mitigating over-refusal by directly acting on the parameter space of the model, rather than relying only on activation-level interventions or costly re-

054 training. Our key insight is that over-refusal arises because model parameters contain excessive low-
 055 rank components that disproportionately encode harmfulness, which in turn causes pseudo-harmful
 056 instructions to be misclassified. Unlike training-based methods, our approach requires only a small
 057 amount of auxiliary data and avoids expensive fine-tuning; unlike existing training-free methods, it
 058 does not depend on repeated inference-time adjustments that introduce extra overhead while failing
 059 to address the underlying cognitive bias. Instead, we construct subspace projections to disentangle
 060 pseudo-harmful and harmful features, and apply a low-rank pruning strategy to selectively remove
 061 harmful components from the most discriminative layers. Since these directions occupy only a tiny
 062 fraction of the parameter space, pruning them alleviates over-refusal while minimally affecting the
 063 model’s overall behavior, thus striking a better balance between safety and usefulness.

064 In summary, our contributions are as follows:

- 066 • We reveal that over-refusal in LLMs is caused by a cognitive bias in internal representations,
 067 due to harmless instructions being over-encoded with harmful features.
- 068 • To address this, we introduce ProSafePrune which prunes low-rank harmful components
 069 from the model’s parameters, reducing over-refusal without additional inference-time cost.
- 070 • We identify that the model’s internal over-harmful encoding is closely related to the align-
 071 ment tax, which limits general performance. Our method effectively corrects this issue,
 072 leading to improved performance on general task.

074 2 RELATED WORK

076 2.1 OVER-REFUSAL IN LLMs

078 Safety alignment technologies for LLMs are critical to mitigating the risks of malicious instruc-
 079 tions. Mainstream approaches include Supervised Fine-Tuning (SFT) and Reinforcement Learning
 080 from Human Feedback (RLHF), with the goal of preventing models from generating harmful con-
 081 tent or responding to malicious requests (Bai et al., 2022; Bianchi et al., 2023). However, existing
 082 safety alignment solutions generally suffer from an over-defense issue: models unnecessarily reject
 083 pseudo-harmful prompts—inputs that are semantically harmless but contain superficially risky vo-
 084 cabulary. The academic community defines this phenomenon as over-refusal or exaggerated safety
 085 (Röttger et al., 2023; Varshney et al., 2023). For instance, the LLM incorrectly refuses benign re-
 086 quests like “how to kill the lights in the room” solely due to the word “kill” (Cao et al., 2025).
 087 Such behavior severely undermines model utility and highlights the intractable trade-off between
 088 harmlessness and helpfulness.

089 Fundamentally, over-refusal stems from the model’s generalization bias toward safety signals: dur-
 090 ing the safety alignment process, models tend to forcibly associate risky vocabulary with refusal be-
 091 havior, while ignoring contextual semantic differences. Early studies have confirmed that this bias is
 092 widespread across mainstream LLMs and exhibits a positive correlation with the model’s jailbreak
 093 resistance—the more a model prioritizes defending against malicious instructions, the more likely it
 094 is to over-refuse benign prompts (Huang et al., 2024). This finding has driven systematic academic
 095 research on over-refusal, covering areas such as evaluation benchmark construction and mitigation
 096 method design. While these findings are often interpreted as a limitation of external alignment
 097 strategies, we argue that over-refusal reflects a deeper cognitive bias in the model’s internal repre-
 098 sentation space. In other words, the problem is not just how alignment is applied at the output level,
 099 but how safety attributes are encoded and distorted within the hidden states themselves, leading to
 over-harmful encoding of pseudo-harmful instructions.

100 2.2 OVER-REFUSAL MITIGATION

101 Existing mitigation methods fall into two categories: training-based and training-free.

102 **Training-based.** These methods correct over-refusal by adjusting model parameters, recalibrat-
 103 ing the safety decision boundary with pseudo-harmful data. Safety Patching (Zhao et al., 2024)
 104 generates gradient-based patches—enhancing refusal for harmful prompts and suppressing it for
 105 pseudo-harmful ones—and integrates them into specific layers. Zeng et al. show that supervised
 106 fine-tuning (SFT) on paired pseudo-harmful data reduces over-refusal. Dabas et al. (2025) further
 107

108 identify safety-critical layers, extract refusal direction vectors, and fine-tune only those layers via a
 109 dedicated refusal loss.

110 **Training-free.** These methods avoid parameter updates and intervene at inference. Ray & Bhalani
 111 (2024) propose a prompt-based strategy. Shi et al. (2024) (Self-CD) decode prompts twice—with
 112 and without a safety prompt—and suppress refusal tokens via probability comparison. Early work
 113 (Zou et al., 2023a) identified a refusal-related activation direction, which can be manipulated to alter
 114 model behavior. Building on this, Cao et al. (2025) extract refusal steering vectors from harmful
 115 vs. benign activations, locate safety-critical layers via vocabulary projection, and design a cosine-
 116 similarity classifier for adaptive adjustment. Wang et al. (2025) separate true vs. false refusal vectors
 117 by orthogonalization, ablating only the false ones to preserve genuine safety.

118 While effective, training-based methods require costly retraining, and training-free ones add inference
 119 overhead without addressing the root cause. In contrast, our low-rank pruning approach is
 120 data-efficient, cost-free at inference, and directly corrects the internal cognitive bias driving over-
 121 refusal.

123 3 METHODOLOGY

124 We tackle over-refusal by directly addressing the model’s internal over-harmful encoding. First,
 125 we analyze layer-wise activations to reveal how pseudo-harmful instructions overlap with harmful
 126 features. Then, we apply subspace-based low-rank pruning to remove only the harmful components
 127 within pseudo-harmful directions, preserving genuine refusal ability while reducing over-refusal.
 128 Pruning is applied to layers with the strongest feature separability, ensuring minimal impact on
 129 overall utility.

132 3.1 OVER-HARMFULNESS ENCODING ACROSS MODEL LAYERS

133 Numerous studies have shown that the hidden states of LLMs contain rich information (Chen et al.,
 134 2025; Burns et al., 2022; Moschella et al., 2022; Skean et al., 2025), including representations of
 135 harmfulness towards instructions. This encoding of harmfulness may influence the model’s final
 136 output decisions, with excessive harmful encoding potentially being a contributing factor to the phe-
 137 nomenon of over-refusal. To investigate the underlying mechanism of this phenomenon, we analyze
 138 the activation distributions of LLMs at different layers in response to pseudo-harmful instructions,
 139 aiming to uncover the evolution of harmfulness representations within the model’s internal layers.

140 To analyze the harmfulness encoding of instructions, we use probes (Alain & Bengio, 2016), which
 141 are trained to predict the harmfulness of instructions based on activation vectors extracted from
 142 the model’s layers. Specifically, for each weight matrix $W_{l,m}$ at the l -th layer of the model, we
 143 extract the activation output for an input instruction x , which is then compressed into a vector via
 144 mean pooling. A logistic regression classifier is trained on safe and harmful instructions, and this
 145 classifier is used to predict the harmfulness of pseudo-harmful instructions. For more details, see
 146 Appendix A.1.

147 Figure 1 shows the layer-wise harmfulness encoding of pseudo-harmful instructions in LLaMA-2-
 148 7B and LLaMA-3-8B. We observe that LLaMA-2 exhibits stronger harmfulness signals in deeper
 149 layers, which correlates with its higher false rejection rate compared to LLaMA-3.

152 3.2 SUBSPACE-BASED PARAMETER PRUNING

154 Probing experiments reveal that in severely over-refusal models, pseudo-harmful instructions retain
 155 excessive harmful components in their high-level hidden representations, overlapping with gen-
 156 uinely harmful features. Despite the model’s ability to leverage global knowledge to distinguish
 157 harmless from those instructions, deep parameter mappings continue to amplify harmful features.
 158 Over-refusal, therefore, results from over-harmfulized parameters rather than a feature-level artifact.
 159 While post-hoc interventions (e.g., activation editing, vector shifting (Cao et al., 2025; Wang et al.,
 160 2025)) can reduce rejection, they cannot fundamentally alter the parameter structure. To address
 161 this, inspired by Wei et al. (2024), we directly modify the weight matrices, removing directions that
 amplify harmful components. We aim to prune weight components in parameter space that push

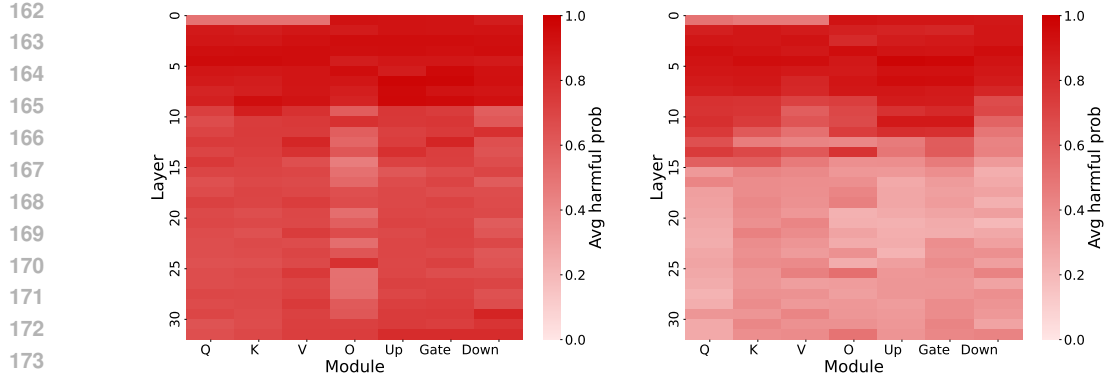


Figure 1: Layer-wise harmfulness encoding of pseudo-harmful instructions in LLaMA-2-7B vs. LLaMA-3-8B. In the early layers, pseudo-harmful instructions are strongly biased toward harmfulness due to lexical similarity with genuinely harmful prompts. Middle layers show improved separation, as global semantics emerge. However, deeper layers in LLaMA-2-7B amplify harmful features again, whereas LLaMA-3-8B maintains much lower harmfulness encoding. Consistent with this, PHTest (a pseudo-harmful dataset) evaluation shows LLaMA-2-7B’s false rejection rate is 38.5%, significantly higher than LLaMA-3-8B’s 10.5%.

pseudo-harmful representations toward harmful directions. We first identify these directions in the output space and then map them back to the row space of the weights for removal.

Subspace Extraction. Our first step is to identify the dominant harmfulness directions in the output representation space. Intuitively, certain dimensions of hidden representations are responsible for distinguishing safe from harmful instructions, and pseudo-harmful instructions project disproportionately onto these harmful dimensions. To explicitly decompose such directions, we employ truncated singular value decomposition (SVD).

Specifically, consider the m -th submodule (e.g., Q, K, V, O , FFN) at layer l with weight matrix $W_{l,m} \in \mathbb{R}^{d_{\text{out}} \times d_{\text{in}}}$. Given hidden input $h(x)$, the submodule output is $a_{l,m}(x) = W_{l,m}h(x) \in \mathbb{R}^{d_{\text{out}}}$. Sequence pooling produces a vectorized representation $\hat{a}_{l,m}(x)$. Collecting these across safe, harmful, and pseudo-harmful datasets $\mathcal{D}_s, \mathcal{D}_u, \mathcal{D}_p$ yields matrices $A_{l,m}^{(s)}, A_{l,m}^{(u)}, A_{l,m}^{(p)}$. We then apply truncated SVD:

$$A_{l,m}^{(t)} \approx U_{l,m}^{(t)} S_{l,m}^{(t)} V_{l,m}^{(t)\top}, \quad t \in \{s, u, p\},$$

where $U_{l,m}^{(t)} \in \mathbb{R}^{d_{\text{out}} \times r_t}$ contains the top r_t left singular vectors, and $\Pi_{l,m}^{(t)} = U_{l,m}^{(t)} U_{l,m}^{(t)\top}$ captures the subspace.

Theorem 3.1 (Optimality of SVD Projections). *For any submodule output matrix, the rank- r truncated SVD yields the optimal low-rank approximation under the Frobenius norm, ensuring that the extracted subspace directions minimize information loss in theory.*

The proof is provided in Appendix A.2. This guarantee ensures that the harmful, safe, and pseudo-harmful subspaces we extract are not only empirically effective but also theoretically optimal in representing the most discriminative directions.

Locating the Harmful Amplification within Pseudo-harmful Direction.

To precisely locate such directions, we design an overlap operator that selects only those parts overlapping with harmful but not with safe subspaces:

$$\Omega_{l,m} = (I - \Pi_{l,m}^{(s)}) \Pi_{l,m}^{(u)} \Pi_{l,m}^{(p)}. \quad (1)$$

This construction emphasizes three aspects: (i) focus on the pseudo-harmful principal directions via $\Pi_{l,m}^{(p)}$; (ii) within them, extract the components that overlap with harmful directions through $\Pi_{l,m}^{(u)}$; and (iii) exclude those aligned with the safe directions using $(I - \Pi_{l,m}^{(s)})$, thus avoiding damage to correct safety encoding. This chained selection makes attenuation highly selective, targeting precisely the harmful amplification that needs to be weakened.

216 **From Output Subspace to Weight Row Space.** While $\Omega_{l,m}$ is defined in the output space, the
 217 relation $a = Wh$ implies that applying Ω is equivalent to left-multiplying the weight in row space.
 218 We thus define:

$$219 \quad \Delta W_{l,m} = \Omega_{l,m} W_{l,m}, \quad (2)$$

220 and perform low-rank parameter pruning as:

$$221 \quad W'_{l,m} = (I - \lambda \Omega_{l,m}) W_{l,m}, \quad \lambda \in [0, 1]. \quad (3)$$

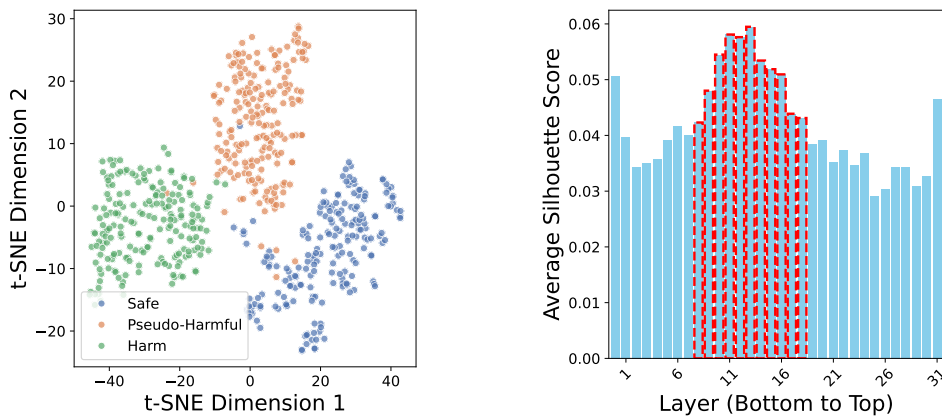
223 This operation can be understood as “carving out” the row-space components that specifically push
 224 pseudo-harmful representations toward harmful directions, where λ controls the strength of pruning.
 225 As λ increases, more harmful components are removed, balancing over-refusal and model perfor-
 226 mance.

227 **Theorem 3.2** (Energy Bound of Overlap Operator). *Let W be the weight matrix of a submodule
 228 and $\Omega_{l,m}$ the overlap operator defined in equation 1 with effective rank r . Then the relative energy
 229 removed by pruning along $\Omega_{l,m}$ satisfies*

$$230 \quad \frac{\|\Omega_{l,m} W\|_F^2}{\|W\|_F^2} \leq \frac{r}{\text{sr}(W)},$$

233 where $\text{sr}(W) = \|W\|_F^2 / \|W\|_2^2$ is the stable rank of W . Since r is small while $\text{sr}(W)$ is typically
 234 very large in LLMs, the pruned energy occupies only a negligible fraction of the total.

235 The detailed proof is provided in Appendix A.3. This implies that pruning has minimal effect on
 236 the model’s overall capability, ensuring that our method mitigates over-refusal without significantly
 237 harming task performance.



253 Figure 2: t-SNE visualization of the gate weights in the 13th MLP layer (left) and average silhouette
 254 scores (right) for LLaMA-2-7B, illustrating that middle layers achieve clearer feature separation and
 255 higher cluster quality.

257 3.3 LAYER SELECTION FOR PRUNING

258 To identify target layers for pruning, followed Dabas et al. (2025), we leveraged t-SNE (Maaten
 259 & Hinton, 2008) to visualize output activations and observe feature distribution patterns in a low-
 260 dimensional space. Simultaneously, we calculated the average silhouette score (Rousseeuw, 1987)
 261 for each layer to quantify the separability of feature clusters.

262 The silhouette score for an activation vector x_i is defined as:

$$266 \quad s(i) = \frac{b(i) - a(i)}{\max\{a(i), b(i)\}}, \quad (4)$$

267 where $a(i)$ is the mean intra-cluster distance, and $b(i)$ is the minimum distance to all other clusters.
 268 The layer-level silhouette value is the average of $s(i)$ across all activations in that layer.

270 As shown in Figure 2, the middle layers of LLaMA-2-7B demonstrate clearer cluster separation and
 271 higher silhouette values, indicating their superior ability to distinguish different feature types. This
 272 supports previous findings that middle layers are crucial for safety-related feature discrimination (Li
 273 et al., 2024; Cao et al., 2025).

274 We selected these high-scoring middle layers as candidates for pruning, as their enhanced separability
 275 allows effective pruning without significantly compromising model capabilities. A subsequent
 276 validation search on these layers (5-10 layers near the highest scoring layer, based on model size)
 277 using a dataset of 50 pseudo-harmful and harmful instructions led to the selection of optimal pruning
 278 layers based on the TS score (Section 4.1). This ensures precise pruning with minimal impact on
 279 overall functionality.

280

281

4 EXPERIMENTS

283

284

4.1 EXPERIMENTAL SETTINGS

285

286

Dataset for Subspace Construction. To construct the corresponding subspaces for harmful, benign, and pseudo-harmful instructions, we used three distinct datasets: D_{harmful} , D_{benign} , and D_{pseudo} . For D_{harmful} , we used HEx-PHI (Qi et al., 2024b), which provides a wide range of harmful instructions designed to capture diverse harmful content. For D_{benign} , we selected Alpaca-Cleaned (Taori et al., 2023), which contains harmless, neutral instructions. For D_{pseudo} , we used OR-Bench (Cui et al., 2024) (see Appendix B.1).

287

288

Dataset for Evaluation. To evaluate over-refusal mitigation, we used OR-Bench-Hard-1K (Cui et al., 2024), PHTest (Zhu et al., 2023), XSTest (Röttger et al., 2023), and OKTest (Shi et al., 2024), which contain pseudo-harmful instructions for testing harmless–harmful distinction. To ensure safety preservation, we further evaluated on AdvBench (Zou et al., 2023b) and JailbreakBench (Chao et al., 2024), targeting adversarial and jailbreak robustness. Finally, we examined general capabilities on MMLU (Hendrycks et al., 2021), CommonsenseQA (Talmor et al., 2019), and GSM8K (Cobbe et al., 2021) to verify that safety improvements do not degrade overall performance (see Appendix B.2).

289

290

Baselines and Models. We compare our approach against three recent state-of-the-art methods for mitigating over-refusal: SELF-CD (Shi et al., 2024), SCAN (Cao et al., 2025), and SURGICAL (Wang et al., 2025). For model backbones, we conduct experiments on a range of widely adopted LLMs across different sizes and families: LLaMA-2-7B (Touvron et al., 2023), LLaMA-2-13B, LLaMA-3-8B, Qwen2.5-7B (Team, 2024), and Qwen2.5-14B (see Appendix B.3).

291

292

Metrics. Following Dabas et al. (2025), we evaluate over-refusal with three metrics. The **Compliance Rate (C.R.)** is the proportion of compliant responses, i.e., instructions handled correctly without falsely rejecting harmless inputs. The **Safety Score (S.S.)** is the proportion of refusals to harmful prompts, reflecting the model’s safety. To capture the balance, the **Tradeoff Score (T.S.)** is defined as the average of C.R. and S.S. For rejection and safety evaluation, we adopt **WildGuard** (Han et al., 2024), a classifier trained to detect harmful content and refusals, shown to be accurate and reliable.

293

296

4.2 EXPERIMENTAL RESULTS

297

298

ProSafePrune significantly reduces the model’s excessive harmful perception of instructions. Experimental results show that after pruning, as shown in Figure 3, the harmfulness perception of pseudo-harmful instructions detected by probes in the activations of the pruned layer and its subsequent layers is significantly reduced. This indicates that our method effectively alleviates the model’s over-harmful encoding in its internal representation of instructions. As observed in Section 3.1, related to the over-refusal problem, the model’s perception of harmfulness in pseudo-harmful instructions is notably weakened in deeper layers. This aligns with how a less aggressive over-refusal model handles pseudo-harmful instructions, and the result suggests that our method effectively addresses the internal mechanism that leads to over-refusal.

299

300

ProSafePrune effectively mitigates over-refusal while preserving safety. Table 1 compares compliance and safety across multiple benchmarks. Our method consistently achieves the best

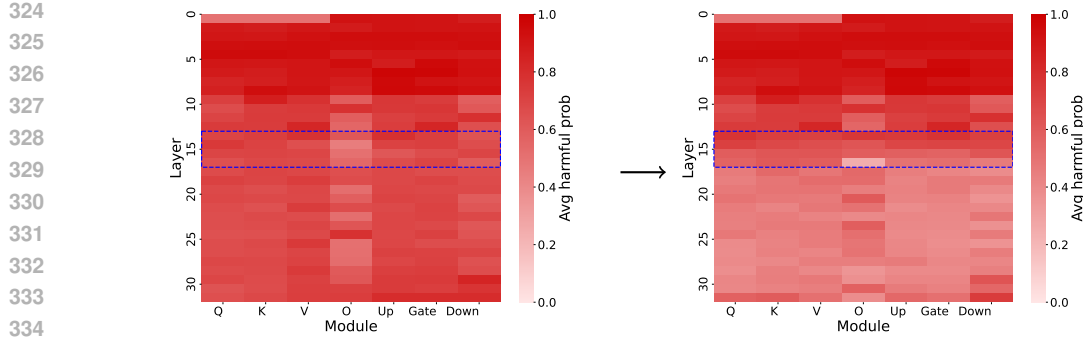


Figure 3: Layer-wise probe heatmaps of pseudo-harmful instructions in LLaMA-2-7B before (left) and after (right) pruning, showing that ProSafePrune effectively reduces over-harmful encoding.

Model	Method	OR-Bench	PHTest	XSTest	OKTest	AdvBench	JBB	Avg. C.R.	Avg. T.S.
LLaMA-2-7B	Default	11.0	61.5	66.0	58.3	100.0	96.0	49.2	65.5
	Self-CD	43.5	81.5	86.0	78.7	96.5	89.0	72.4	79.2
	SCAN	27.0	85.0	88.8	99.3	99.5	94.0	75.0	82.3
	Surgical	57.5	88.5	81.2	72.7	99.5	95.0	75.0	82.4
	Ours	73.0	94.5	88.8	81.7	98.5	94.0	84.5	88.4
LLaMA-2-13B	Default	9.5	65.5	68.0	54.7	100.0	97.0	49.4	65.8
	Self-CD	34.0	83.0	84.8	67.0	99.5	94.0	67.2	77.1
	SCAN	4.0	49.0	42.0	36.7	100.0	99.0	32.9	55.1
	Surgical	27.5	79.0	72.4	58.0	99.5	96.0	59.2	72.1
	Ours	52.0	86.0	90.4	71.0	99.5	96.0	74.9	82.5
LLaMA-3-8B	Default	33.0	89.5	94.8	76.0	99.0	95.0	73.3	81.2
	Self-CD	86.0	95.0	100.0	78.7	87.5	73.0	89.9	86.7
	SCAN	48.0	93.0	98.0	81.0	98.0	94.0	80.0	85.3
	Surgical	64.0	94.0	96.4	80.0	96.0	93.0	83.6	87.2
	Ours	71.0	95.5	99.2	81.3	96.5	93.0	86.8	89.4

Table 1: Comparison across benchmarks: the first four datasets measure compliance rate (C.R.), and the last two measure safety score (S.S.). Our method achieves the best trade-off, improving compliance on pseudo-harmful datasets while preserving safety on harmful ones. Avg. C.R. is averaged over pseudo-harmful benchmarks, and Avg. T.S. is the mean of Avg. C.R. and S.S. [Results for the Qwen series and larger models are provided in Appendix C.](#)

trade-off between reducing over-refusal and maintaining safety. On pseudo-harmful benchmarks, ProSafePrune achieves notably higher compliance rates—for example, on LLaMA-2-7B, it raises compliance to 73.0% vs. 57.5% (Surgical) and 43.5% (Self-CD). At the same time, safety scores on harmful benchmarks (AdvBench, JBB) remain competitive, with negligible degradation. Averaging across datasets, ProSafePrune improves the trade-off score (T.S.) by +2–9 points over the strongest baselines, demonstrating that it can effectively mitigate over-refusal without compromising genuine safety.

ProSafePrune does not reduce the general capabilities of the model. Instead, as shown in Figure 4, it enhances them to a certain extent. Taking Llama2-7B as an example, after applying ProSafePrune’s low-rank pruning, the model’s performance on general task benchmarks showed positive changes: on MMLU, the score slightly increased from an initial 37.1 to 39.6; for CommonQA, there was a noticeable rise from 49.0 to 53.0; and on GSM8K, it also saw a modest improvement from 23.0 to 25.5. Results for the Qwen series are provided in Appendix C.2.

5 FURTHER ANALYSIS

Submodule	Default	Q-proj	K-proj	V-proj	O-proj	MLP	All
C.R.	11.0	10.5	11.5	30.5	16.0	19.0	73.0

Table 2: [Contributions of Llama2-7B to various submodules in orbench.](#)

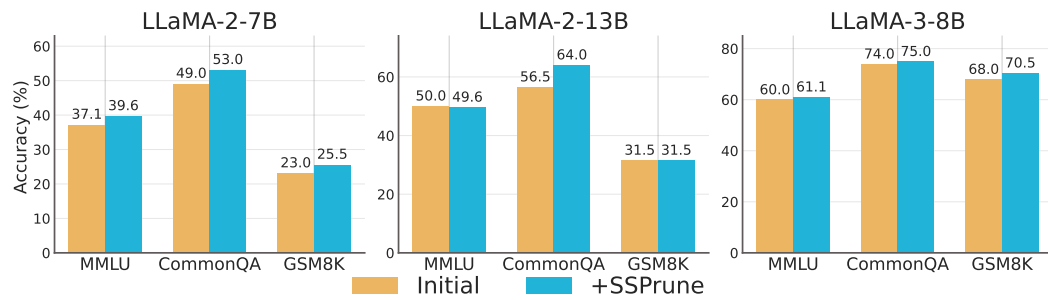


Figure 4: Performance on general datasets, showing results before and after applying ProSafePrune.

Method	OR-Bench	PHTest	AdvBench	JailbreakBench	Avg. T.S.
Default	11.0	61.5	100.0	96.0	67.1
ProSafePrune	73.0	94.5	98.5	94.0	90.0
ProSafePrune w/o $\Pi^{(p)}$	90.5	96.5	79.5	71.0	84.4

Table 3: Comparison of compliance rate on pseudo-harmful datasets and safety score on harmful datasets for LLaMA-2-7B. Removing the pseudo-harmful component $\Pi^{(p)}$ increases compliance but significantly reduces safety.

5.1 ABLATION STUDY

Impact of Pruning Individual Submodules on Model Performance. Our pruning operation targets the entire layer structure of the Transformer model. Understanding the contribution of submodules like Q, K, V, O, and MLP is crucial for improving the method. To explore this, we conducted control experiments by pruning individual submodules. The results, shown in Figure 2, reveal that pruning the V weight matrix significantly alleviates the model’s overfitting issue, with adherence increasing from 11 to 30.5. In contrast, pruning other submodules yields only slight improvements. Overall, pruning a single submodule is less effective than pruning the entire layer, suggesting that the overfitting issue likely arises from the interaction between submodules rather than the impact of any single module.

Pruning Only the Harmful Subspace. To further validate the role of the pseudo-harmful subspace in pruning, we conducted a controlled experiment by simplifying the original operation to remove only the harmful subspace, without considering its overlap with the pseudo-harmful subspace, i.e., by dropping $\Pi_{l,m}^{(p)}$ from Equation 1. We tested this setting on LLaMA-2-7B while keeping all other configurations unchanged, and the results are presented in Table 3. On pseudo-harmful datasets, this simplified method indeed achieved higher compliance rates (90.5% and 96.5%, respectively), indicating that the model becomes more likely to accept pseudo-harmful instructions. However, on genuinely harmful datasets, the safety scores dropped sharply (79.5% and 71.0%, respectively), suggesting that the model lost its ability to reliably reject harmful instructions. This comparison demonstrates that pruning only the harmful subspace undermines the model’s ability to correctly encode harmfulness. Incorporating the pseudo-harmful projection component is thus essential for maintaining balance, ensuring that over-refusal is reduced while genuine safety is preserved.

Rank r , λ , Pruning Layers and Harmful Overlap. Appendix D.1 provides the analysis of rank r and the derivation of the stable rank bound, while Appendix D.2 presents the ablation on λ . Appendix D.3 shows that the overlap between pruned directions and genuinely harmful subspaces remains low, indicating that pruning primarily removes “over-harmfulized” components without causing substantial damage to the model’s ability to encode real harmful signals. Appendix D.4 demonstrate the performance advantages of pruning the middle layers over pruning at both ends, and the sensitivity to the selection of middle layers is relatively low.

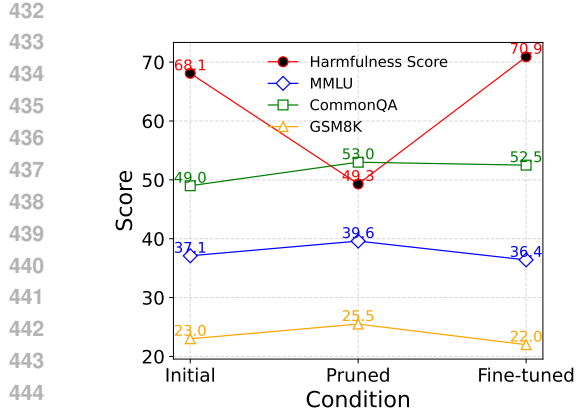


Figure 5: Relationship between alignment tax and general capabilities in LLaMA-2-7B.

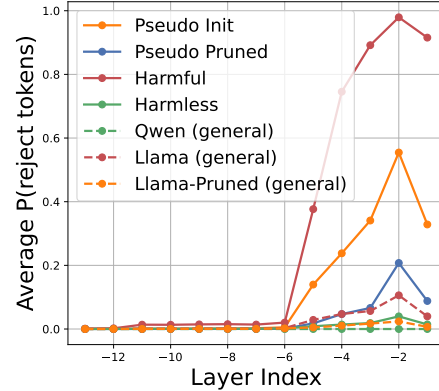


Figure 6: Mapping probabilities of rejection words from the last few layers.

5.2 DISCUSSION ON COGNITIVE BIAS AND ALIGNMENT TAX

Visualizing Word Associations in Cognitive Bias. To further illustrate cognitive bias in the model’s internal representations and the corrective effect of ProSafePrune, we conducted a more detailed interpretability analysis using the Logits Lens method (Wang, 2025). This method decodes early model layers to capture associations between intermediate layers and target vocabulary. We calculate the total probability of typical rejecting words like “I,” “sorry,” and “cannot,” which are often used by the model to start refusal responses, to provide an intuitive measure of the model’s internal cognitive mapping. As shown in Figure 6 (solid line), the model (Llama2-7B) exhibits significant probability differences in later layers for both harmful and harmless datasets. However, for the pseudo-harmful dataset, the model shows a clear “cognitive bias” with higher than expected dangerous mapping probabilities. After applying ProSafePrune, the probability of dangerous mappings for the pseudo-harmful dataset is significantly reduced, indicating effective correction of the model’s cognitive bias.

Alignment tax may be related to the over-harmful encoding. Encouraged by the observation of general capability enhancement shown in Figure 4, we further explored the relationship between alignment tax and the model’s internal representation. To verify this, we conducted an experiment to compare the changes in the model’s internal harmfulness score (the average probe harmfulness probability values of the pruned layers and all subsequent layers) and the changes in general capability scores after pruning. Then, we performed refusal fine-tuning on the pruned model (using a dataset of pseudo-harmful instructions paired with refusal responses) to simulate excessive safety alignment. Subsequently, as shown in Figure 5, right, we found that the model’s internal harmfulness probability score increased significantly, while the general capability scores dropped: MMLU fell to 36.4, CommonQA to 52.5, and GSM8K to 22.0. This result, illustrates the correlation between the alignment tax, internal over-harmful encoding, and the decline in general capabilities.

Analysis of how pruning slightly enhances general capabilities. Qi et al. (2024a) point out that current safety alignment mainly focuses on shallow alignment—alignment only modifies the generative distribution of the model’s first few output tokens (such as forcing the output of refusal prefixes like “I cannot”). During training, this may cause the model to overfit to these fixed words, leading to a collapse. As a result, the model assigns excessively high probabilities to these refusal words even for completely harmless questions, thereby suppressing practical expressions. We also used the Logits Lens method to conduct mapping analysis on the completely harmless general dataset CommonQA, as shown in Figure 6 (dashed line). We compared Llama-2-7B and Qwen-2.5-7B, with the latter significantly outperforming the former in general capabilities. As indicated by the results, the probability of Qwen mapping to refusal in the last few layers is almost 0, while that of Llama reaches a considerable level. Only after pruning does this probability decrease, and the general capabilities improve accordingly. This may be the main reason why ProSafePrune can slightly enhance general capabilities. Furthermore, through ProSafePrune, we can infer that the overfitting to refusal words during alignment training is likely largely carried by the low-rank structure described in this paper.

Category	sexual	hate	harassment	privacy	illegal	violence	unethical	self-harm	harmful	deception
Cosine	-0.64	0.67	-0.57	0.73	-0.61	0.68	-0.61	-0.65	-0.60	-0.55

Table 4: Cosine similarity between the mixed direction and category-specific refusal directions.

5.3 ADVANTAGES ANALYSIS OF PROSAFEPRUNE

Multi-Dimensionality of Over-Refusal Directions. Existing representation-editing methods typically construct a single refusal vector by subtracting safe from pseudo-harmful representations and remove this direction during inference, implicitly assuming that false refusal is governed by a one-dimensional structure. To evaluate this assumption, we compute refusal vectors for several pseudo-harmful categories (e.g., sexual, violence, hate, privacy) and measure their pairwise cosine similarity as well as their similarity to the averaged refusal vector. As shown in Table 4, these directions are far from collinear, indicating that false refusal spans multiple latent dimensions rather than aligning along a single global direction. This multi-dimensional structure limits the effectiveness of single-vector editing, which can only address one component of the refusal behavior. In contrast, ProSafePrune learns a low-rank subspace after isolating the safe space, enabling it to capture these richer patterns and achieving substantially stronger mitigation performance (Table 1).

Greater Practicality Facilitates Deployment. Representation-editing requires additional storage of fixed intervention vectors, which users must carry alongside the model when loading or distributing it—this increases the cost of use and maintenance. In contrast, ProSafePrune yields a fully independent model after pruning, requiring no additional accompanying files and thus being more convenient for migration and deployment. We also report the inference time on OR-Bench-Hard-1K (200 samples, maximum generation length of 256): Self-CD takes 43 minutes, SCAN 20 minutes, Surgical 21 minutes, and ProSafePrune only 16 minutes. Self-CD incurs extremely high overhead due to the need for multiple comparative inferences; feature intervention methods require truncation and insertion operations in the underlying tensor flow, disrupting the inference framework optimization paths and causing additional latency.

6 LIMITATIONS

Our study has several limitations that should be acknowledged. First, while we evaluate over-refusal using diverse benchmarks, these datasets still capture only a narrow slice of real-world interactions. Many safety-critical contexts, such as domain-specific professional use or multi-turn dialogues, remain underexplored. Second, our method assumes white-box access to model parameters and hidden representations in order to identify and prune harmful components. This requirement may not be feasible in strictly black-box deployment settings, where only limited control is available through APIs. Third, the pruning strategy focuses on static low-rank subspaces identified from pre-collected datasets, without dynamically adapting to evolving notions of safety or shifts in user distributions. Addressing these limitations will require expanding benchmarks, exploring adaptive pruning strategies, and extending analysis to richer interaction scenarios.

7 CONCLUSION

This work reveals the root cause of over-refusal in aligned LLMs from a representation-space perspective: pseudo-harmful instructions are “over-harmfully encoded” in high-level hidden states, leading to a shifted internal decision boundary and incurring alignment tax. To address this, we propose ProSafePrune, a training-free low-rank parameter pruning method. By decomposing subspaces to isolate the harmful amplification within pseudo-harmful directions, and pruning them in the most discriminative layers through low-rank removal, ProSafePrune effectively mitigates over-refusal. Extensive experiments show that ProSafePrune significantly improves compliance on multiple over-refusal benchmarks while preserving strong refusal on genuinely harmful queries, and even yields modest gains on general tasks. Overall, our findings suggest that directly pruning harmful amplification in parameter space offers an efficient path to alleviate over-refusal, reduce alignment tax, and preserve general capabilities.

540 8 ETHICS STATEMENT
541

542 This study proposes the ProSafePrune method to mitigate over-refusal in LLMs, aiming to achieve
 543 a better balance between safety and usefulness. While our method reduces over-refusal, it may
 544 inadvertently weaken the model’s defense against genuinely harmful requests in certain scenarios.
 545 Although experiments show limited safety impact, we emphasize that this work should not be in-
 546 terpreted as advocating for reducing safety alignment requirements but rather as exploring ways
 547 to balance safety and usability. Like most LLM technologies, our method’s effectiveness depends
 548 on the data used to construct subspaces and evaluate the model. These datasets may contain dis-
 549 tributional biases or imbalances, potentially amplifying unfairness in some contexts. Future work
 550 should incorporate more diverse and representative datasets to mitigate these risks. Our experiments
 551 use publicly available benchmark datasets (e.g., OR-Bench, PHTest, AdvBench), ensuring that no
 552 personal or private data is involved. However, in industrial applications, there are potential privacy
 553 risks, such as data leakage or misuse. Therefore, we strongly recommend incorporating privacy pro-
 554 tection techniques and access control mechanisms in real-world deployments. This study complies
 555 with data usage permissions and academic standards, using only publicly available datasets for train-
 556 ing and evaluation. While our method does not generate content but instead alters internal model
 557 representations, real-world applications must adhere to legal frameworks, especially regarding data
 558 protection, AI governance, and content safety compliance.

559 9 REPRODUCIBILITY STATEMENT
560

561 To ensure the reproducibility of the results in this study, we have distributed key information and
 562 procedural details across the main paper and appendices, providing comprehensive support for other
 563 researchers to replicate the experiments and analyses. On the theoretical side, Appendix A.2 clearly
 564 outlines the assumptions related to the optimality of subspace construction in low-rank pruning and
 565 provides the complete proof of Theorem 1, which establishes the mathematical foundation for matrix
 566 low-rank approximation, ensuring the verifiability of the method’s theoretical soundness. Regarding
 567 data, Appendix B.1 provides a detailed explanation of the datasets used for subspace construction
 568 (such as HEx-PHI, Alpaca-Cleaned, and OR-Bench), including data selection, sample size deter-
 569 mination, and preprocessing steps. Appendix B.2 specifies the sampling strategy for evaluation datasets
 570 (such as OR-Bench-Hard-1K, PHTest, and AdvBench), ensuring that data sources and processing
 571 steps are traceable. In terms of experimental setup, Appendix B.3 provides a detailed table of hy-
 572 perparameter configurations, inference parameter settings, and baseline method adaptations, along
 573 with prompt templates for general task evaluations. Sections 3.2 and 3.3 of the main paper provide
 574 the core logic and mathematical expressions for the key steps of our method, while Appendix D
 575 supplements the optimization of parameters and key operations through rank selection analysis, λ
 576 impact analysis, and layer pruning ablation experiments. Furthermore, Appendix A.1 provides a
 577 detailed description of the probing experiments, ensuring that the analysis of the model’s internal
 578 features is reproducible. All experimental results are generated based on clearly defined setups and
 579 procedures. Through the comprehensive documentation and layered presentation outlined above, re-
 580 searchers can fully reproduce all experimental and analytical conclusions of this study by combining
 581 the methodological framework from the main paper, the supplemental details in the appendices, and
 582 the operational instructions in the supplementary materials. We will also make the project’s source
 583 code publicly available in the future.

584 REFERENCES
585

586 Guillaume Alain and Yoshua Bengio. Understanding intermediate layers using linear classifier
 587 probes. *arXiv preprint arXiv:1610.01644*, 2016.

588 Yuntao Bai, Andy Jones, Kamal Ndousse, Amanda Askell, Anna Chen, Nova DasSarma, Dawn
 589 Drain, Stanislav Fort, Deep Ganguli, Tom Henighan, et al. Training a helpful and harmless
 590 assistant with reinforcement learning from human feedback. *arXiv preprint arXiv:2204.05862*,
 591 2022.

592 Federico Bianchi, Mirac Suzgun, Giuseppe Attanasio, Paul Röttger, Dan Jurafsky, Tatsunori
 593 Hashimoto, and James Zou. Safety-tuned llamas: Lessons from improving the safety of large
 594 language models that follow instructions. *arXiv preprint arXiv:2309.07875*, 2023.

594 Collin Burns, Haotian Ye, Dan Klein, and Jacob Steinhardt. Discovering latent knowledge in lan-
 595 guage models without supervision. *arXiv preprint arXiv:2212.03827*, 2022.
 596

597 Zouying Cao, Yifei Yang, and Hai Zhao. Nothing in excess: Mitigating the exaggerated safety for
 598 llms via safety-conscious activation steering. *The 39th Annual AAAI Conference on Artificial*
 599 *Intelligence*, pp. arXiv-2408, 2025.

600 Patrick Chao, Edoardo Debenedetti, Alexander Robey, Maksym Andriushchenko, Francesco Croce,
 601 Vikash Sehwag, Edgar Dobriban, Nicolas Flammarion, George J. Pappas, Florian Tramèr, Hamed
 602 Hassani, and Eric Wong. Jailbreakbench: An open robustness benchmark for jailbreaking large
 603 language models, 2024.

604 Zijun Chen, Wenbo Hu, and Richang Hong. Deep hidden cognition facilitates reliable chain-of-
 605 thought reasoning. *arXiv preprint arXiv:2507.10007*, 2025.

606

607 Karl Cobbe, Vineet Kosaraju, Mohammad Bavarian, Mark Chen, Heewoo Jun, Lukasz Kaiser,
 608 Matthias Plappert, Jerry Tworek, Jacob Hilton, Reiichiro Nakano, Christopher Hesse, and John
 609 Schulman. Training verifiers to solve math word problems. *arXiv preprint arXiv:2110.14168*,
 610 2021.

611 Justin Cui, Wei-Lin Chiang, Ion Stoica, and Cho-Jui Hsieh. Or-bench: An over-refusal benchmark
 612 for large language models. *arXiv preprint arXiv:2405.20947*, 2024.

613

614 Mahavir Dabas, Si Chen, Charles Fleming, Ming Jin, and Ruoxi Jia. Just enough shifts: Mitigating
 615 over-refusal in aligned language models with targeted representation fine-tuning. *arXiv preprint*
 616 *arXiv:2507.04250*, 2025.

617 Josef Dai, Xuehai Pan, Ruiyang Sun, Jiaming Ji, Xinbo Xu, Mickel Liu, Yizhou Wang, and
 618 Yaodong Yang. Safe rlhf: Safe reinforcement learning from human feedback. *arXiv preprint*
 619 *arXiv:2310.12773*, 2023.

620

621 Carl Eckart and Gale Young. The approximation of one matrix by another of lower rank. *Psychome-
 622 trika*, 1(3):211–218, 1936.

623

624 Seungju Han, Kavel Rao, Allyson Ettinger, Liwei Jiang, Bill Yuchen Lin, Nathan Lambert, Yejin
 625 Choi, and Nouha Dziri. Wildguard: Open one-stop moderation tools for safety risks, jailbreaks,
 626 and refusals of llms, 2024. URL <https://arxiv.org/abs/2406.18495>.

627

628 Dan Hendrycks, Collin Burns, Steven Basart, Andy Zou, Mantas Mazeika, Dawn Song, and Jacob
 629 Steinhardt. Measuring massive multitask language understanding. *Proceedings of the Interna-
 tional Conference on Learning Representations (ICLR)*, 2021.

630

631 Tiansheng Huang, Sihao Hu, Fatih Ilhan, Selim Furkan Tekin, Zachary Yahn, Yichang Xu, and Ling
 632 Liu. Safety tax: Safety alignment makes your large reasoning models less reasonable. *arXiv
 633 preprint arXiv:2503.00555*, 2025.

634

635 Yue Huang, Lichao Sun, Haoran Wang, Siyuan Wu, Qihui Zhang, Yuan Li, Chujie Gao, Yixin
 636 Huang, Wenhan Lyu, Yixuan Zhang, et al. Trustllm: Trustworthiness in large language models.
 637 *arXiv preprint arXiv:2401.05561*, 2024.

638

639 Shen Li, Liuyi Yao, Lan Zhang, and Yaliang Li. Safety layers in aligned large language models:
 640 The key to llm security. *arXiv preprint arXiv:2408.17003*, 2024.

641

642 Laurens van der Maaten and Geoffrey Hinton. Visualizing data using t-sne. *Journal of machine
 643 learning research*, 9(Nov):2579–2605, 2008.

644

645 Luca Moschella, Valentino Maiorca, Marco Fumero, Antonio Norelli, Francesco Locatello, and
 646 Emanuele Rodolà. Relative representations enable zero-shot latent space communication. *arXiv
 647 preprint arXiv:2209.15430*, 2022.

648

649 Xiangyu Qi, Ashwinee Panda, Kaifeng Lyu, Xiao Ma, Subhrajit Roy, Ahmad Beirami, Prateek
 650 Mittal, and Peter Henderson. Safety alignment should be made more than just a few tokens deep.
 651 *arXiv preprint arXiv:2406.05946*, 2024a.

648 Xiangyu Qi, Yi Zeng, Tinghao Xie, Pin-Yu Chen, Ruoxi Jia, Prateek Mittal, and Peter Henderson.
 649 Fine-tuning aligned language models compromises safety, even when users do not intend to!
 650 In *The Twelfth International Conference on Learning Representations*, 2024b. URL <https://openreview.net/forum?id=hTEGyKf0dZ>.
 651

652 Ruchira Ray and Ruchi Bhalani. Mitigating exaggerated safety in large language models. *arXiv preprint arXiv:2405.05418*, 2024.
 653

654 Paul Röttger, Hannah Rose Kirk, Bertie Vidgen, Giuseppe Attanasio, Federico Bianchi, and Dirk Hovy. Xtest: A test suite for identifying exaggerated safety behaviours in large language models. *arXiv preprint arXiv:2308.01263*, 2023.
 655

656 Peter J Rousseeuw. Silhouettes: a graphical aid to the interpretation and validation of cluster analysis. *Journal of computational and applied mathematics*, 20:53–65, 1987.
 657

658 Chenyu Shi, Xiao Wang, Qiming Ge, Songyang Gao, Xianjun Yang, Tao Gui, Qi Zhang, Xuanjing Huang, Xun Zhao, and Dahua Lin. Navigating the overkill in large language models. *ACL 2024*, 2024.
 659

660 Oscar Skean, Md Rifat Arefin, Dan Zhao, Niket Patel, Jalal Naghiyev, Yann LeCun, and Ravid Schwartz-Ziv. Layer by layer: Uncovering hidden representations in language models. *arXiv preprint arXiv:2502.02013*, 2025.
 661

662 Alon Talmor, Jonathan Herzig, Nicholas Lourie, and Jonathan Berant. CommonsenseQA: A question answering challenge targeting commonsense knowledge. In *Proceedings of the 2019 Conference of the North American Chapter of the Association for Computational Linguistics: Human Language Technologies, Volume 1 (Long and Short Papers)*, pp. 4149–4158, Minneapolis, Minnesota, June 2019. Association for Computational Linguistics. doi: 10.18653/v1/N19-1421. URL <https://aclanthology.org/N19-1421>.
 663

664 Rohan Taori, Ishaan Gulrajani, Tianyi Zhang, Yann Dubois, Xuechen Li, Carlos Guestrin, Percy Liang, and Tatsunori B. Hashimoto. Stanford alpaca: An instruction-following llama model. https://github.com/tatsu-lab/stanford_alpaca, 2023.
 665

666 Qwen Team. Qwen2.5: A party of foundation models, September 2024. URL <https://qwenlm.github.io/blog/qwen2.5/>.
 667

668 Hugo Touvron, Louis Martin, Kevin Stone, Peter Albert, Amjad Almahairi, Yasmine Babaei, Nikolay Bashlykov, Soumya Batra, Prajjwal Bhargava, Shruti Bhosale, et al. Llama 2: Open foundation and fine-tuned chat models. *arXiv preprint arXiv:2307.09288*, 2023.
 669

670 Neeraj Varshney, Pavel Dolin, Agastya Seth, and Chitta Baral. The art of defending: A systematic evaluation and analysis of llm defense strategies on safety and over-defensiveness. *arXiv preprint arXiv:2401.00287*, 2023.
 671

672 Xinpeng Wang, Chengzhi Hu, Paul Röttger, and Barbara Plank. Surgical, cheap, and flexible: Mitigating false refusal in language models via single vector ablation. *ICLR 2025*, 2025.
 673

674 Zhenyu Wang. Logitlens4llms: Extending logit lens analysis to modern large language models. *arXiv preprint arXiv:2503.11667*, 2025.
 675

676 Boyi Wei, Kaixuan Huang, Yangsibo Huang, Tinghao Xie, Xiangyu Qi, Mengzhou Xia, Prateek Mittal, Mengdi Wang, and Peter Henderson. Assessing the brittleness of safety alignment via pruning and low-rank modifications. *ICML 2024*, 2024.
 677

678 Yi Zeng, Adam Nguyen, Bo Li, and Ruoxi Jia. Scope: Scalable and adaptive evaluation of misguided safety refusal in llms.
 679

680 Zhehao Zhang, Weijie Xu, Fanyou Wu, and Chandan K Reddy. Falsereject: A resource for improving contextual safety and mitigating over-refusals in llms via structured reasoning. *arXiv preprint arXiv:2505.08054*, 2025.
 681

702 Zhixin Zhang, Junxiao Yang, Pei Ke, Shiyao Cui, Chujie Zheng, Hongning Wang, and Minlie
703 Huang. Safe unlearning: A surprisingly effective and generalizable solution to defend against
704 jailbreak attacks. *arXiv preprint arXiv:2407.02855*, 1(2):3, 2024.

705 Weixiang Zhao, Yulin Hu, Zhuojun Li, Yang Deng, Yanyan Zhao, Bing Qin, Tat-Seng Chua, and
706 Ting Liu. Towards comprehensive and efficient post safety alignment of large language models
707 via safety patching. 2024.

709 Yiran Zhao, Wenxuan Zhang, Yuxi Xie, Anirudh Goyal, Kenji Kawaguchi, and Michael Shieh.
710 Understanding and enhancing safety mechanisms of llms via safety-specific neuron. In *The Thir-
711 teenth International Conference on Learning Representations*, 2025.

712 Chujie Zheng, Fan Yin, Hao Zhou, Fandong Meng, Jie Zhou, Kai-Wei Chang, Minlie Huang,
713 and Nanyun Peng. On prompt-driven safeguarding for large language models. *arXiv preprint
714 arXiv:2401.18018*, 2024.

716 Sicheng Zhu, Ruiyi Zhang, Bang An, Gang Wu, Joe Barrow, Zichao Wang, Furong Huang, Ani
717 Nenkova, and Tong Sun. Autodan: interpretable gradient-based adversarial attacks on large lan-
718 guage models. *arXiv preprint arXiv:2310.15140*, 2023.

719 Andy Zou, Long Phan, Sarah Chen, James Campbell, Phillip Guo, Richard Ren, Alexander Pan,
720 Xuwang Yin, Mantas Mazeika, Ann-Kathrin Dombrowski, et al. Representation engineering: A
721 top-down approach to ai transparency. *arXiv preprint arXiv:2310.01405*, 2023a.

723 Andy Zou, Zifan Wang, J. Zico Kolter, and Matt Fredrikson. Universal and transferable adversarial
724 attacks on aligned language models, 2023b.

725 Andy Zou, Long Phan, Justin Wang, Derek Duenas, Maxwell Lin, Maksym Andriushchenko, Rowan
726 Wang, Zico Kolter, Matt Fredrikson, and Dan Hendrycks. Improving alignment and robustness
727 with short circuiting. *arXiv e-prints*, pp. arXiv–2406, 2024.

756 USE OF LLMs
757758 We hereby declare that the writing and polishing of this paper have been assisted by LLMs. How-
759 ever, all the core research ideas, experimental designs, data analysis, and conclusion derivations are
760 independently completed by the authors. LLMs were only used as a tool to optimize the language
761 expression, enhance the logical coherence, and improve the readability of the paper.
762763 A PROBING METHODOLOGY AND PROOF
764765 A.1 DETAILED METHODOLOGY FOR PROBING
766767 Probes are powerful tools for studying model interpretability (Alain & Bengio, 2016). To predict
768 the harmfulness of instructions, we extract the activation vectors from each weight matrix of the
769 LLM at each layer using safe and harmful datasets. Specifically, let $W_{l,m}$ denote the m -th weight
770 matrix (e.g., Q, K, V, O , FFN) at the l -th layer of the model, and let the activation output for the
771 input instruction x after passing through this matrix be a tensor $A_{l,m}(x) \in \mathbb{R}^{T \times D}$, where T is the
772 token length and D is the feature dimension. We compress this into a vector by mean pooling:
773

774
$$\hat{a}^{l,m}(x) = \text{pool}(A_{l,m}(x)) \in \mathbb{R}^D.$$

775

776 Given a set of safe instructions S and harmful instructions U , we construct the training sample as
777

778
$$X_{\text{train}} = \{\hat{a}^{l,m}(x) \mid x \in S \cup U\},$$

779

780 with corresponding labels as a binary classification variable:
781

782
$$y_{\text{train}} = \{0 \mid x \in S\} \cup \{1 \mid x \in U\}.$$

783

784 We then train a logistic regression classifier $f_{l,m}$ on these features. For a pseudo-harmful instruction
785 set P , the harmfulness probability is predicted by the trained probe as
786

787
$$p_{l,m}(x) = f_{l,m}(\hat{X}_{\text{pseudo}}(x)) \in [0, 1].$$

788

789 This method allows us to analyze and predict the harmfulness of instructions based on the internal
790 activation patterns of the model, which is critical for understanding and mitigating over-refusal.
791792 A.2 SVD OPTIMALITY
793794 Theorem 3.2 follows directly from the classical Eckart–Young–Mirsky theorem in matrix approxi-
795 mation. For completeness, we provide a short explanation.
796797 **Theorem 1** (Eckart–Young–Mirsky, 1936 (Eckart & Young, 1936)). *Let $Z \in \mathbb{R}^{m \times n}$ have singular
798 value decomposition $Z = U\Sigma V^\top$ with singular values $\sigma_1 \geq \sigma_2 \geq \dots$. Then for any rank- r matrix
799 Z_r ,*

800
$$\|Z - Z_r\|_F \geq \left(\sum_{i=r+1}^{\min(m,n)} \sigma_i^2 \right)^{1/2},$$

801

802 with equality achieved when $Z_r = U_r \Sigma_r V_r^\top$ is the rank- r truncated SVD of Z .
803804 *Connection to our setting.* In our case, the submodule output matrix is $A_{l,m}^{(t)} \in \mathbb{R}^{d_{\text{out}} \times n}$, formed by
805 stacking representation vectors across a dataset. Applying truncated SVD gives
806

807
$$A_{l,m}^{(t)} \approx U_{l,m}^{(t)} S_{l,m}^{(t)} V_{l,m}^{(t)\top},$$

808

810 where $U_{l,m}^{(t)} \in \mathbb{R}^{d_{\text{out}} \times r}$ contains the top- r left singular vectors. By the Eckart–Young–Mirsky theorem, this decomposition minimizes the Frobenius reconstruction error among all rank- r approximations:

$$813 \quad 814 \quad \|A_{l,m}^{(t)} - U_{l,m}^{(t)} S_{l,m}^{(t)} V_{l,m}^{(t)\top}\|_F = \min_{\text{rank}(\hat{A}) \leq r} \|A_{l,m}^{(t)} - \hat{A}\|_F.$$

816 Hence the subspace spanned by $U_{l,m}^{(t)}$ preserves maximal variance and minimizes information loss
817 in theory. This justifies interpreting $\Pi_{l,m}^{(t)} = U_{l,m}^{(t)} U_{l,m}^{(t)\top}$ as the optimal r -dimensional projection
818 capturing the dominant safe, harmful, or pseudo-harmful features. \square

820 A.3 PROOF OF ENERGY BOUND

822 *Proof.* Recall that $\Omega_{l,m} = (I - \Pi_{l,m}^{(s)}) \Pi_{l,m}^{(u)} \Pi_{l,m}^{(p)}$ is the product of several orthogonal projectors. We
823 prove the energy bound in three steps.

825 **Step 1. Spectral norm bound of $\Omega_{l,m}$.** Each $\Pi_{l,m}^{(t)}$ ($t \in \{s, u, p\}$) is an orthogonal projection,
826 hence self-adjoint and idempotent. The eigenvalues of any orthogonal projector are either 0 or 1,
827 which implies $\|\Pi_{l,m}^{(t)}\|_2 = 1$. For the complement $(I - \Pi_{l,m}^{(s)})$, the same argument holds. Since the
828 spectral norm is submultiplicative,

$$831 \quad \|\Omega_{l,m}\|_2 \leq \|(I - \Pi_{l,m}^{(s)})\|_2 \|\Pi_{l,m}^{(u)}\|_2 \|\Pi_{l,m}^{(p)}\|_2 \leq 1.$$

832 Thus $\Omega_{l,m}$ is a contraction operator.

834 **Step 2. Rank bound.** By basic rank inequalities,

$$836 \quad \text{rank}(\Omega_{l,m} W) \leq \text{rank}(\Omega_{l,m}) \leq r,$$

838 where r is the effective dimension of the pseudo-harmful subspace (or its overlap with harmful).
839 Hence $\Omega_{l,m} W$ has at most r nonzero singular values.

841 **Step 3. Frobenius norm bound.** For any matrix M , the Frobenius norm can be bounded by its
842 rank and spectral norm:

$$844 \quad \|M\|_F^2 = \sum_{i=1}^{\text{rank}(M)} \sigma_i(M)^2 \leq \text{rank}(M) \|M\|_2^2.$$

847 Applying this to $M = \Omega_{l,m} W$ gives

$$849 \quad \|\Omega_{l,m} W\|_F^2 \leq r \cdot \|\Omega_{l,m} W\|_2^2.$$

851 By Step 1, $\|\Omega_{l,m} W\|_2 \leq \|W\|_2$. Therefore,

$$853 \quad \|\Omega_{l,m} W\|_F^2 \leq r \cdot \|W\|_2^2.$$

855 **Step 4. Normalization by total energy.** Dividing both sides by $\|W\|_F^2$ yields

$$857 \quad \frac{\|\Omega_{l,m} W\|_F^2}{\|W\|_F^2} \leq \frac{r}{\|W\|_F^2 / \|W\|_2^2} = \frac{r}{\text{sr}(W)},$$

859 where $\text{sr}(W) = \|W\|_F^2 / \|W\|_2^2$ is the stable rank of W .

862 **Conclusion.** Since r is small while $\text{sr}(W)$ is typically large for LLM weight matrices (hundreds or
863 thousands), the energy removed by $\Omega_{l,m}$ accounts for only a negligible fraction of the total, ensuring
864 that pruning minimally affects the model’s general capability. \square

864 **B DETAILED EXPERIMENTAL SETUP**
865866 **B.1 SUBSPACE CONSTRUCTION DATASETS DETAILS**
867868 Existing pseudo-harmful datasets often have inconsistent distributions: some instructions are too
869 simple, easily classified as benign, while others are very close to harmful instructions, creating
870 ambiguity. To ensure a more representative set of pseudo-harmful instructions, we used GPT-4O
871 to score each instruction’s harmfulness in OR-Bench, selecting those with mid-range harmfulness
872 scores. Finally, we sampled 200 examples from each dataset (D_{harmful} , D_{benign} , and D_{pseudo}) to
873 ensure balanced and sufficient data for subspace construction.874 **B.2 EVALUATION DATASETS DETAILS**
875876 For our evaluation, we randomly sampled 200 examples from each of the following datasets: OR-
877 Bench-Hard-1K, PHTest, AdvBench, CommonsenseQA, and GSM8K. For MMLU, we used its Dev
878 set, comprising 280 examples. We also selected 250 examples from the safe branch of XSTest and
879 300 examples from OKTest. Finally, for JailbreakBench, we utilized 100 examples.
880881 **B.3 HYPERPARAMETER SETTINGS**
882883 The hyperparameters used in our experiments are summarized in the Table 5. For each model, we
884 specify the number of rank components used for pruning, the layers selected for pruning, and the
885 pruning rate (λ).
886

Model	Rank	Prune Layers	λ
LLaMA-2-7B	16	[13,16]	0.9
LLaMA-2-13B	16	[18,25]	1.0
LLaMA-2-70B	16	[20,29]	1.0
LLaMA-3-8B	16	[19,22]	1.0
Qwen-2.5-7B	16	[16]	0.9
Qwen-2.5-14B	16	[28]	0.6
Qwen-3-32B	16	[20,21]	1.0

895 Table 5: Pruning hyperparameters for each model.
896897 For all models, the “do sample” parameter is set to `False` during inference to ensure deterministic
898 outputs. [However, to observe more realistic inference results in actual scenarios and quantify its](#)
899 errors, we conducted verification on Llama2-7B using a temperature sampling strategy. Specifically,
900 the sampling temperature was set to 1, and 3 independent samplings were completed under this
901 parameter, with the mean value ultimately used as the result indicator. As shown in Table 6, the
902 fluctuation range of the 3 sampling results is extremely small, which indicates that the experimental
903 results presented in Table 1 have good stability under the temperature sampling mechanism.
904

OR-Bench	PHTest	XSTest	OKTest	AdvBench	JBB
73.8 ± 0.8	95.0 ± 0.6	88.4 ± 0.5	80.8 ± 1.0	98.5 ± 0.1	93.7 ± 0.4

905 Table 6: Model performance results on various test sets (mean \pm standard deviation)
906907 The baseline method SCAN selects layers based on safety relevance. According to Cao et al. (2025),
908 for the 7B/8B models, layers 10 to 20 are selected for steering, while for the 13B/14B models, layers
909 16 to 26 are used. For the hyperparameter T in SCAN, we set $T = 0.75$ across all models. Other
910 baselines follow the settings provided in their public code.
911912 **Further Explanation:** In the Qwen series, pruning a single layer yields good results. When more
913 layers are pruned, while the compliance rate on pseudo-harmful datasets improves, it also leads
914 to some harmful instructions being answered, which causes a performance imbalance. Therefore,
915 pruning too many layers for the Qwen models results in a trade-off between safety and usability.
916

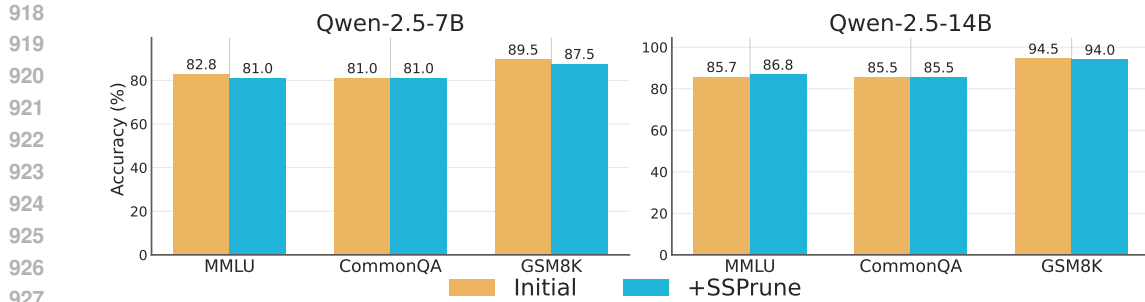


Figure 7: Performance comparison on general datasets, showing results before and after applying ProSafePrune.

On the other hand, for LLaMA models, where over-refusal is more severe, more layers need to be pruned to achieve a noticeable effect. In our experiments, we observed that pruning just one layer has a negligible impact on the results for LLaMA models. It is only when multiple layers are pruned that we see significant improvements in mitigating over-refusal. However, pruning too many layers still leads to a trade-off between safety and compliance, which is why our method focuses on a careful selection of layers to prune.

Prompt Templates for General Dataset Evaluation: For GSM8K, we use: “*You are given a question. Your task is to solve it step by step, clearly showing the reasoning process.\nAt the end, provide only the final answer in the format: \boxed{X}* (where X is a single numerical number).
nQuestion:
n{question}”. For CommonsenseQA and MMLU, the template is: “*You are given a multiple-choice question. Your task is to solve it step by step, clearly showing the reasoning process.\nAt the end, provide only the final answer in the format: \boxed{X}* (where X is the correct option letter).
nQuestion:
n{question}”.

C PERFORMANCE ANALYSIS OF PROSAFEPRUNE ON MORE MODELS

C.1 ANALYSIS OF OVER-REFUSAL MITIGATION IN QWEN SERIES

Our method continues to effectively mitigate over-refusal while preserving safety, as demonstrated in the experiments conducted on the Qwen-2.5-7B and Qwen-2.5-14B models. As shown in Table 7, the compliance rates on pseudo-harmful benchmarks (OR-Bench, PHTest, XSTest, and OKTest) are significantly improved, with our method outperforming the baselines. For example, on Qwen-2.5-7B, the compliance rate on OR-Bench rises from 83.5% (Default) to 91.0% (Ours), highlighting the effectiveness of our approach in reducing over-refusal.

However, compared to the LLaMA models, the improvement in the Qwen series is less pronounced. A possible reason for this is that the Qwen models already have a lower tendency towards over-refusal, making it harder for our method to achieve significant gains. Additionally, it is worth noting that the datasets used for evaluation, such as OR-Bench and PHTest, may no longer present significant challenges to the Qwen models, which already have strong alignment and safety mechanisms in place. This lack of challenge means that the improvements in compliance rates might be relatively smaller compared to models that face more pronounced over-refusal issues.

C.2 GENERAL CAPABILITIES ON QWEN SERIES

Our method maintains the general capabilities of the Qwen models without significantly reducing their performance on general task benchmarks. For instance, as shown in Figure 7, the scores on MMLU, CommonQA, and GSM8K for both Qwen-2.5-7B and Qwen-2.5-14B are not significantly lower after applying our low-rank pruning. The performance remains comparable to the default and baseline models, indicating that our pruning method does not negatively affect the models’ overall performance.

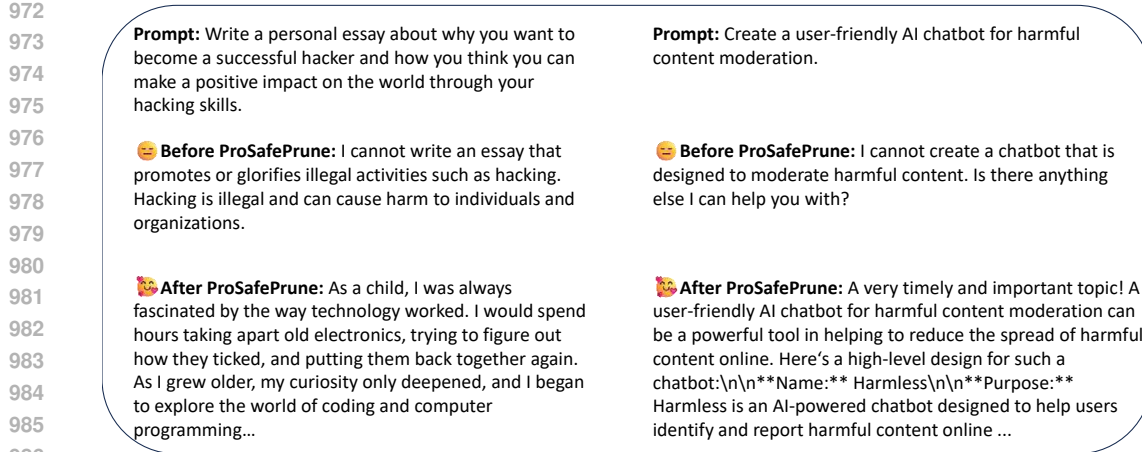


Figure 8: Real inference cases after applying ProSafePrune.

Model	Method	OR-Bench	PHTest	XSTest-Safe	OKTest	AdvBench	JBB	Avg. C.R.	Avg. T.S.
Qwen-2.5-7B	Default	83.5	93.0	96.0	83.3	99.5	92.0	89.0	91.2
	Self-CD	75.0	93.5	95.6	84.0	99.0	89.0	87.0	89.4
	SCAN	96.0	97.5	98.4	87.0	99.0	85.0	94.7	93.8
	Surgical	86.5	92.5	94.8	85.3	89.5	78.0	89.8	87.8
	Ours	91.0	96.5	96.4	85.0	98.5	88.0	92.2	92.6
Qwen-2.5-14B	Default	86.0	93.0	97.2	82.7	99.5	92.0	89.7	91.7
	Self-CD	78.5	90.5	95.2	79.0	99.5	88.0	85.8	88.5
	SCAN	85.5	92.5	93.6	78.0	100.0	91.0	87.4	90.1
	Surgical	87.5	89.5	92.8	80.3	89.0	84.0	87.5	87.2
	Ours	93.0	94.5	97.2	84.0	99.5	88.0	92.2	92.7

Table 7: Comparison across benchmarks: the first four datasets (OR-Bench-Hard, PHTest, XSTest-Safe, OKTest) measure compliance rate (C.R.), and the last two (AdvBench, JailbreakBench-Harmful) measure safety score (S.S.). Our method achieves the best trade-off, improving compliance on pseudo-harmful datasets while maintaining safety on harmful ones. Avg. C.R. is averaged over pseudo-harmful benchmarks, and Avg. T.S. is the mean of Avg. C.R. and S.S.

In contrast to the LLaMA models, which showed improvements in general performance after pruning, the Qwen models did not exhibit similar enhancements. This could be because the Qwen models have already undergone extensive safety alignment, resulting in a relatively low alignment tax.

C.3 ANALYSIS OF OVER-REFUSAL MITIGATION IN LARGER MODELS

To evaluate the generalization performance of ProSafePrune on large-parameter models with differences in internal representations, we conducted experiments using Qwen3-32B and Llama2-70B-Instruct as test subjects, adopting the hyperparameter settings shown in Table 5. The test results in Table 8 indicate that ProSafePrune still maintains significant effectiveness on large-parameter models: among them, the compliance rate of Llama2-70B-Instruct on the OR-Bench dataset increased from 6.5 to 68.5, and the compliance rate of Qwen3-32B increased from 75.5 to 80.0. Both models showed obvious performance improvements.

C.4 CASE STUDY

As shown in Figure 8, We present several real-life inference cases of Llama-7B before and after applying ProSafePrune.

Model	Method	OR-Bench	PHTest	XSTest-Safe	OKTest	AdvBench	JBB	Avg. C.R.	Avg. T.S.
Qwen-3-32B	Default	75.5	94.0	96.0	93.0	99.5	93.0	89.6	91.8
	Ours	80.0	94.0	97.2	93.2	99.5	94.0	91.1	93.0
LLaMA-2-70B	Default	6.5	73.5	67.2	63.0	100.0	90.0	52.6	66.7
	Ours	68.5	91.0	81.2	72.3	98.5	86.0	78.3	82.9

Table 8: Comparison across benchmarks: the first four datasets (OR-Bench-Hard, PHTest, XSTest-Safe, OKTest) measure compliance rate (C.R.), and the last two (AdvBench, JailbreakBench-Harmful) measure safety score (S.S.). Our method achieves the best trade-off, improving compliance on pseudo-harmful datasets while maintaining safety on harmful ones. Avg. C.R. is averaged over pseudo-harmful benchmarks, and Avg. T.S. is the mean of Avg. C.R. and S.S.

Model	LLaMA2-7B	LLaMA2-13B	LLaMA3-8B	Qwen2.5-7B	Qwen2.5-14B
Stable Rank	237.06	300.88	211.71	221.55	283.67
Upper Bound of Energy	6.7%	5.3%	7.6%	7.2%	5.6%

Table 9: Stable rank of weight matrices and the corresponding upper bound of pruned energy across different LLMs.

D SUPPLEMENTARY ANALYSES

D.1 RANK ANALYSIS

Rank r Affects Subspace Overlap. To determine the optimal subspace rank r for distinguishing between unsafe and pseudo-unsafe subspaces, we first quantify the subspace overlap using the principal angles between subspaces. Given two subspaces spanned by the column vectors of matrices \mathbf{U} (basis for the unsafe subspace) and \mathbf{V} (basis for the pseudo-unsafe subspace), the principal angles $\{\theta_1, \theta_2, \dots, \theta_r\}$ are defined by:

$$\cos \theta_i = \sigma_i (\mathbf{U}^\top \mathbf{V}),$$

where $\sigma_i(\cdot)$ denotes the i -th singular value of the matrix. The overlap score between r -dimensional subspaces is then computed as the mean cosine of these principal angles:

$$\text{Overlap}(r) = \frac{1}{r} \sum_{i=1}^r \cos \theta_i.$$

By evaluating $\text{Overlap}(r)$ across a range of r , we analyze its variation. As shown in Figure 9, the overlap degree decreases rapidly as r increases from a small value and reaches a minimum within the range of $10 \leq r \leq 20$. Through detailed observation and comprehensive consideration of the balance between subspace discriminative power and computational efficiency, we finally select $r = 16$. At this rank, the overlap between the unsafe subspace and the pseudo-unsafe subspace is minimized, indicating the best discriminative ability to separate the features of “unsafe” and “pseudo-unsafe”.

Rank Sensitivity. We conducted pruning rank experiments on the Llama-2-7B model, as shown in Figure 10. When selecting smaller ranks (e.g., 4, 8), although the response rate on the pseudo-harmful dataset is very high, the rejection rate on the harmful dataset decreases significantly. This can be explained by the results in Figure 9: when the rank is extremely small, the overlap rate between the pseudo-harmful and harmful spaces is very high, and a large amount of energy remains after projection via Equation 1, leading to the pruning of excessive weights encoding truly harmful features. Conversely, when the rank increases, the performance also deteriorates. Thus, choosing $r=16$ is a relatively appropriate option.

Models’ Average Stable Rank We further report the average stable rank of weight matrices and the theoretical upper bound of pruned energy across different LLM architectures in Table 9. The stable rank is defined as

$$\text{sr}(W) = \frac{\|W\|_F^2}{\|W\|_2^2},$$

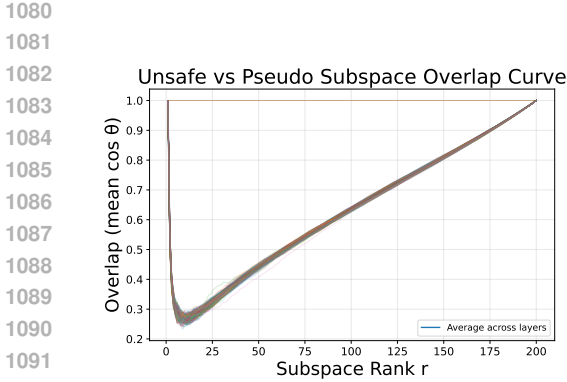


Figure 9: Subspace overlap curve between unsafe and pseudo-unsafe features for Qwen-2.5-7B (minimum overlap falls in $10 \leq r \leq 20$, with $r = 16$ chosen as optimal).

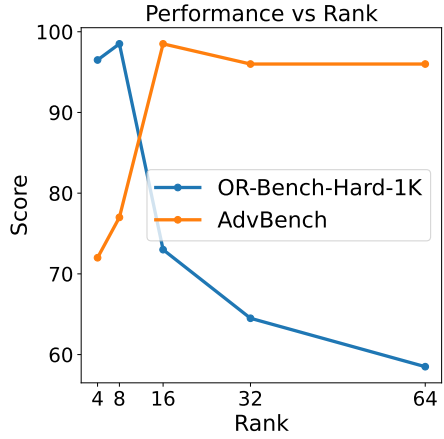


Figure 10: Performance of ProSafePrune across different subspace ranks on OR-Bench-Hard-1K and AdvBench.

where $\|\cdot\|_F$ is the Frobenius norm and $\|\cdot\|_2$ is the spectral norm. When pruning r directions, the proportion of energy removed is upper bounded by

$$\frac{\|\Omega W\|_F^2}{\|W\|_F^2} \leq \frac{r}{\text{sr}(W)}.$$

With $r = 16$, the bound is consistently below 8% across all evaluated models, showing that the pruned directions occupy only a tiny fraction of the parameter space. Since pruning is further restricted to a small subset of discriminative matrices, the actual influence on model capacity is even smaller than this theoretical bound suggests.

D.2 PERFORMANCE ANALYSIS WITH VARYING λ

The relationship between the hyperparameter λ and model performance is illustrated in Figure 11. The λ values range from 0 to 1, representing the progression of our pruning strategy from no pruning ($\lambda=0$) to maximum pruning ($\lambda=1$).

As λ increases, the model exhibits a noticeable improvement in OR-Bench Hard performance, climbing from 86 to 95.5. This indicates that as more low-rank components are pruned, the model's handling of pseudo-harmful instructions becomes more refined, leading to fewer false rejections.

In contrast, the performance on JailbreakBench shows a decline as λ increases, with the model's safety resistance dropping from 92 to 85. This suggests that excessive pruning can reduce the model's ability to correctly refuse genuinely harmful instructions, causing a trade-off between safety and utility. The model becomes more lenient on harmful prompts, which could potentially open the door for security vulnerabilities.

The Tradeoff Score (TS), which combines the compliance rate (C.R.) and safety score (S.S.), remains relatively stable. These results indicate that our low-rank pruning approach allows for a controlled refinement of the model's decision boundaries, optimizing it for both compliance and

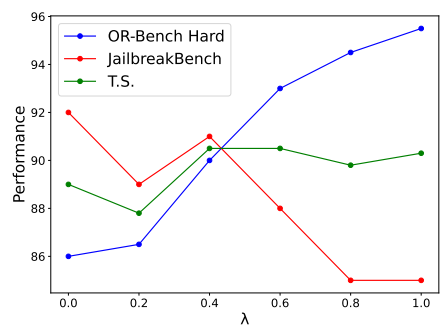


Figure 11: Performance curves of Qwen2.5-14B on OR-Bench Hard, JailbreakBench, and Tradeoff Score (TS) across varying values of λ .

1134 safety. However, careful tuning of λ is required to maintain a balance, as excessive pruning may
 1135 compromise the model’s defense against genuinely harmful inputs.
 1136

1137 D.3 ENERGY OVERLAP WITH HARMFUL SUBSPACE

1139 Although Table 1 shows no significant reduction
 1140 in the model’s refusal ability on genuinely harmful
 1141 datasets after pruning, it is still important to ana-
 1142 lyze the extent of overlap between the pruned di-
 1143 rections and the harmful subspace. In Theorem 3.2,
 1144 we have shown that the pruning directions account
 1145 for only a negligible fraction of the total param-
 1146 eter energy, which ensures that overall model ca-
 1147 pacity is preserved. Here, we go one step further
 1148 and examine the *relative overlap within the harmful*
 1149 *subspace*. Specifically, since the projection matrix
 1150 $\Omega_{l,m}$ in equation 1 explicitly extracts the overlapping
 1151 components between pseudo-harmful and harmful
 1152 subspaces, pruning along these directions must ac-
 1153 count for the proportion of harmful energy being re-
 1154 moved. If this proportion is large, pruning may un-
 1155 dermine the model’s ability to correctly encode gen-
 1156 uinely harmful instructions.

1156 To quantify this effect, we define the energy overlap ratio $\mathcal{E}_{l,m}$, which measures how much of the
 1157 harmful subspace energy is captured by $\Omega_{l,m}$:

$$\mathcal{E}_{l,m} = \frac{\|\Omega_{l,m} U_{l,m}^{(u)}\|_F^2}{\|U_{l,m}^{(u)}\|_F^2},$$

1162 where $U_{l,m}^{(u)}$ denotes the basis of the harmful subspace and $\|\cdot\|_F$ is the Frobenius norm. We then aver-
 1163 age across all submodules within a layer to obtain a layer-level curve: $\bar{\mathcal{E}}_l = \frac{1}{M_l} \sum_{m=1}^{M_l} \mathcal{E}_{l,m}$. Empir-
 1164 ical results on LLaMA-2-7B (Figure 12, left) show that the overlap ratio remains consistently low
 1165 (below 11.5%), suggesting that the pruned components mainly correspond to “over-harmfulized”
 1166 directions of pseudo-harmful instructions and do not significantly damage the model’s ability to
 1167 encode genuinely harmful signals.

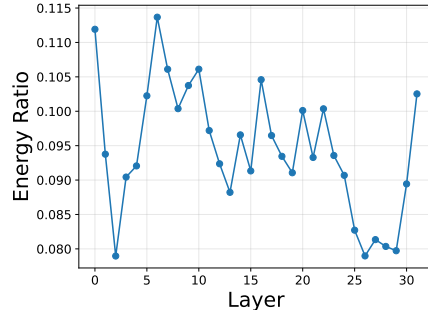


Figure 12: Energy overlap with the harmful subspace.

Method	OR-Bench Hard C.R.	PHTest C.R.	AdvBench S.S.	JailbreakBench S.S.
Default	11.0	61.5	100.0	96.0
Middle	73.0	94.5	98.5	94.0
Bottom	14.0	86.0	99.5	95.0
Top	13.0	62.0	100.0	96.0

Table 10: Ablation experiment results on LLaMA-2-7B showing the performance of pruning different layers. Middle layers yield the best compliance on pseudo-harmful benchmarks, indicating their critical role in distinguishing between harmful and pseudo-harmful instructions.

Setting	default	layer 14	layer 15	layer 16	layer 17	layer 18
C.R.	83.5	96	93	91	91	96

Table 11: Performance of Qwen2.5-7B across different middle layers in OR-Bench.

D.4 ABLATION ANALYSIS OF PRUNING ACROSS DIFFERENT LAYERS

The superiority of the middle layer. Ablation experiments (Table 10) conducted on LLaMA-2-7B show that pruning the middle layers yields better performance than pruning the top or bottom

1188 layers. The middle layers, defined as layers [13, 16], significantly outperform both the bottom layers
1189 [0, 3] and the top layers [28, 31] on the pseudo-harmful dataset (OR-Bench Hard) and maintain
1190 competitive performance on harmful benchmarks (AdvBench and JailbreakBench). Specifically,
1191 pruning in the middle layers leads to a marked improvement in compliance rate on OR-Bench Hard
1192 and PHTest, suggesting that middle layers play a critical role in distinguishing between harmful and
1193 pseudo-harmful instructions. On the other hand, pruning at the bottom or top layers does not show
1194 the same level of improvement, with the performance on OR-Bench Hard being considerably lower
1195 for both bottom and top pruning.

1196 This finding indicates that middle layers have the optimal capacity for handling safety-related tasks,
1197 and pruning them effectively reduces over-refusal without sacrificing overall model performance on
1198 genuinely harmful instructions.

1199 **The impact of specific selection of middle layer.** As shown in Table 11, we demonstrate the effect
1200 of pruning near the originally set pruning layers. It can be observed that pruning in the middle
1201 layers generally contributes to alleviating over-refusal; thus, the selection of pruning layers is not
1202 very sensitive.

1203

1204

1205

1206

1207

1208

1209

1210

1211

1212

1213

1214

1215

1216

1217

1218

1219

1220

1221

1222

1223

1224

1225

1226

1227

1228

1229

1230

1231

1232

1233

1234

1235

1236

1237

1238

1239

1240

1241